Biochimica et Biophysica Acta 1840 (2014) 2935–2943

Contents lists available at ScienceDirect

Biochimica et Biophysica Acta

journal homepage: www.elsevier.com/locate/bbagen

Hydrolytic enzymes conjugated to quantum dots mostly retain whole catalytic activity

Aditya Iyer, Anil Chandra, Rajaram Swaminathan *

Department of Biotechnology, Indian Institute of Technology Guwahati, Guwahati 781039, Assam, India

ARTICLE INFO

Article history:
Received 6 January 2014
Received in revised form 22 May 2014
Accepted 9 June 2014
Available online 14 June 2014

Keywords:
Semiconductor nanocrystals
Hen egg white lysozyme
Alkaline phosphatase
Acetylcholinesterase
Enzyme catalytic activity
Luminescence

ABSTRACT

Background: Tagging a luminescent quantum dot (QD) with a biological like enzyme (Enz) creates value-added entities like quantum dot–enzyme bioconjugates (QDEnzBio) that find utility as sensors to detect glucose or beacons to track enzymes in vivo. For such applications, it is imperative that the enzyme remains catalytically active while the quantum dot is luminescent in the bioconjugate. A critical feature that dictates this is the quantum dot–enzyme linkage chemistry. Previously such linkages have put constraints on polypeptide chain dynamics or hindered substrate diffusion to active site, seriously undermining enzyme catalytic activity. In this work we address this issue using avidin–biotin linkage chemistry together with a flexible spacer to conjugate enzyme to quantum dot.
Methods: The catalytic activity of three biotinylated hydrolytic enzymes, namely, hen egg white lysozyme (HEWL), alkaline phosphatase (ALP) and acetylcholinesterase (AChE) was investigated post-conjugation to streptavidin linked quantum dot for multiple substrate concentrations and varying degrees of biotinylation.
Results: We demonstrate that all enzymes retain full catalytic activity in the quantum dot–enzyme bioconjugates in comparison to biotinylated enzyme alone. However, unlike alkaline phosphatase and acetylcholinesterase, the catalytic activity of hen egg white lysozyme was observed to be increasingly susceptible to ionic strength of medium with rising level of biotinylation. This susceptibility was attributed to arise from depletion of positive charge from lysine amino groups after biotinylation.
Conclusions: We reasoned that avidin–biotin linkage in the presence of a flexible seven atom spacer between biotin and enzyme poses no constraints to enzyme structure/dynamics enabling retention of full enzyme activity.
General significance: Overall our results demonstrate for the first time that streptavidin–biotin chemistry can yield quantum dot enzyme bioconjugates that retain full catalytic activity as native enzyme.

1. Introduction

Quantum dots are tiny (~10 nm) semiconductor nanocrystals that are excellent luminescent labels for biomolecules owing to their bright luminescence in visible-NIR region, size-tunable narrow emission band, superior photostability and broad absorption spectrum for simultaneous excitation of multiple probes in comparison with traditional organic dyes and fluorescent proteins [1]. QDs today find applications in improving photovoltaic devices [2,3], assembling sophisticated biophotonic logic devices [4,5], creating novel thermodynamic machines [6,7] apart from being used for sensing glutathione selectively [8], sensing NO_2 [9], and sensing clenbuterol and melamine [10], as light-emitting devices [11,12] and as active drug tracers *in vivo* [13,14]. Of late, they have also found extensive applications in biology as cellular probes for immunolabeling, multimodal *in vivo* and live animal imaging [15,16], cellular tracking and related applications [17–19].

QD bioconjugates have served as fluorescent labels for both *in vivo* cellular imaging and *in vitro* assay detection [20]. Combining the brightness of QD luminescence with remarkable ligand/substrate recognition specificity of an antibody/enzyme/aptamer has given rise to numerous biomedical applications like sensing glucose [21–23], urea [24], polyphenols [25], and H_2O_2 [26]. Similar conjugates have been useful in detecting toxins like ricin [27], target DNA [28], and cocaine [29] or in monitoring enzyme mediated phosphorylation [30] and release of doxorubicin into cancer cells [31]. Their utility in tracking activity of AChE *in vivo* under diseased conditions [32] or monitoring protein unfolding of human serum albumin [33] has been demonstrated. Such hybrid devices are predicted to find applications in areas ranging from energy harvesting and nanoscale electronics to biomedical diagnostics [34].

Over the past three decades, numerous reports of enzyme conjugated to nanoparticles/nanorods/QDs have appeared (see Table 1). However, in vast majority of such reports, the catalytic activity of enzyme in the conjugate has suffered significant loss rendering them futile. In spite of the diverse number of conjugation strategies employed, there clearly appears no universal method that can guarantee retention of whole enzyme activity in the QDEnzBio conjugate. It is likely that changes in native enzyme conformation, backbone/side-chain dynamics or substrate access to the active site in QDEnzBio might have contributed to

* Corresponding author.
E-mail address: rsw@iitg.ernet.in (R. Swaminathan).

http://dx.doi.org/10.1016/j.bbagen.2014.06.003
0304-4165/

Table 1
Enzyme–nanoparticle conjugates synthesized in the past and their consequence on enzyme activity. Entries are listed in the order they appeared in literature with most recent work reported first.

	Enzyme	Nanoparticle	Conjugation strategy	Inert spacer	Effect on enzyme activity		Reference
1	Tyrosinase (from mushroom)	Glutathione–CdTe QDs	Encapsulated with Poly-(diallyldimethylammonium chloride) in a hybrid film	No	−85%	Decreases	[43]
2	Sialyltransferase (PmST1, from *Pasteurella multocida*)	Magnetic nanoparticles	Cysteine functionalized magnetic NP reacting with protein α-thioester through native chemical ligation	Yes (5 atoms)	−20%	Decreases	[44]
				Yes (23 atoms)	+165%	Increases	
				Yes (45 atoms)	+225%	Increases	
3	Cytidine monophosphate sialic acid synthetase	Magnetic nanoparticles	Cysteine functionalized magnetic NP reacting with protein α-thioester through native chemical ligation	Yes (5 atoms)	−20%	Decreases	
				Yes (23 atoms)	−19%	Decreases	
				Yes (45 atoms)	−14%	Decreases	
4	Sialyltransferase from *Neisseria gonorrhoeae* (NgST) (membrane bound protein)	Magnetic nanoparticles	NgST-Biotin with Streptavidin-magnetic NP	Yes (5 atoms)	−66%	Decreases	
				Yes (23 atoms)	−92%	Decreases	
				Yes (45 atoms)	−82%	Decreases	
5	Type II restriction endonuclease (EcoRI)	CdS QDs	Amide bond using NHS[a] and EDC[b] chemistry	No	Qualitative estimate	No change	[45]
6	Butyrylcholinesterase	3-Mercaptopropionic acid coated CdSe/ZnS QDs	Electrostatic interaction	No	−50%	Decreases	[32]
7	α-Chymotrypsin	Ni nanoparticles	Chemical reduction in aqueous solution	No	−58%	Decreases	[46]
8	Glucose oxidase	CdTe QDs	QD-COOH + GOx-NH_2 with EDC and NHS	No	13 fold lower K_m	Increases	[21]
9	CMP-sialic acid synthetase	Magnetic nanoparticles	Intein expression system and native chemical ligation	Random No	−67%	Decreases	[47]
				Site-specific No	−23%	Decreases	
10	Trypsin	Gold nanorods	Click chemistry (acetylene–trypsin to azide on Au nanorods)	Yes (12 atoms)	−43%	Decreases	[48]
			Amide bond (EDC chemistry)	No	−87%	Decreases more	
			Electrostatic adsorption	No	−81%	Decreases more	
11	α-Chymotrypsin	CdS nanoparticles	Chemical reduction in aqueous solution using TCEP[c]	No	−50%	Decreases	[49]
12	Lipase from *Thermomyces lanuginosus*	Gold nanoparticles	Click chemistry (acetylene–lipase to azide-functionalized Au nanoparticles)	Yes (47 atoms)	0%	No change	[50]
13	Cytochrome $P450_{BS\beta}$	CdS QDs	Electrostatic interaction	No	−83%	Decreases	[51]
14	RNase S	Gold nanoparticles	S-peptide (Cys) with Au NP followed by self-assembly with S-Protein	Yes (3 amino acid peptide spacer)	−99%	Decreases	[52]
15	Pepsin	Colloidal gold	Interaction of Cys–SH or Lys–NH_2 with colloidal gold	No	−19%	Decreases	[53]
16	Aspartic protease from *Aspergillus saitoi*	Colloidal gold	Interaction of Cys–SH or Lys–NH_2 with colloidal gold	No	−10%	Decreases	[54]
17	Horseradish peroxidase	Colloidal gold	Adsorbed to colloidal gold sols that were later electrodeposited onto Pt gauze/glassy carbon	No	Between −7% and −16%	Decreases	[55]
18	Xanthine oxidase	Colloidal gold	Ibid	No	Between −13% and −59%	Decreases	
19	Carbonic anhydrase	Colloidal gold	Ibid	No	−30%	Decreases	
20	Glucose oxidase	Colloidal gold	Ibid	No	Between −20% and −30%	Decreases	

[a] N-hydroxysulfosuccinimide (NHS).
[b] 1-ethyl-3(3-dimethylaminopropyl) carbodiimide hydrochloride (EDC).
[c] Tris(2-carboxyethyl) phosphine hydrochloride (TCEP).

depletion of activity. It has been argued that attaching enzyme to nanoparticles requires control over: ratio of enzyme molecules per nanoparticle, orientation of enzyme on nanoparticle surface, enzyme–nanoparticle separation distance, strength of linkage and universal applicability across multiple enzymes as stated previously [35–38].

In this paper, our objective was to establish a universal approach to conjugate enzyme to quantum dot that specifically ensures *maximum luminescence and catalytic activity* in the conjugate. We chose the avidin–biotin linkage chemistry for this task due to the following reasons: A) The high affinity of biotin–streptavidin interactions are well understood, benign and have emerged as a popular approach to conjugate or link other biological entities like DNA and antibodies to nanoparticles [39–42]. B) This conjugation chemistry is known to be stable over a wide range of pH and has strong salt stability. C) Streptavidin conjugated QDs are commercially available along with kits for biotinylating protein making assembly of QDEnzBio facile. D) The robustness of this interaction among QDEnzBio conjugates is yet to be rigorously tested (Table 1). As the presence of a spacer does seem to improve the enzyme activity at least in a few cases (Table 1), we decided to employ a spacer between enzyme and biotin for this work. Additionally we also decided to vary the substrate concentration and extent of biotinylation on the enzyme to understand the mechanisms that may influence catalytic activity in QDEnzBio.

A systematic analysis of enzyme catalytic rates among the three different enzymes subsequent to conjugation with QDs was therefore undertaken. Enzymes were initially biotinylated with a seven atom spacer separating biotin from enzyme and subsequently conjugated to streptavidin coated QDs. The catalytic rates of the enzymes were measured in aqueous buffers using UV–visible spectrophotometry under: A) multiple substrate concentrations and B) multiple stoichiometries of the biotinylating reagent; both post-biotinylation and post-conjugation to QD.

The three enzymes employed namely, HEWL, ALP and AChE, fall under the enzyme class of hydrolases (EC 3.X.X.X). This particular class of enzymes was chosen because of their predominant use in biosensors and nanosensors warranting the need for the knowledge of their functional stability when conjugated to a QD [56–59]. HEWL (EC 3.2.1.17), a 129 amino acid enzyme is a structurally well characterized protein largely used as food preservative [60]. It is a glycoside hydrolase, which catalyzes hydrolysis of 1,4-beta-linkages between N-acetylmuramic acid and N-acetylglucosamine residues of the peptidoglycan layer of a bacterial cell wall [61]. Recently, HEWL was electrostatically adsorbed to surface of dihydrolipoic acid capped CdSe/ZnS QDs to observe HEWL fibril formation at elevated temperatures in pH 12.5 [62]. ALP (EC 3.1.3.1), which catalyzes the nonspecific hydrolysis of phosphomonoethers, is an essential component of signal transduction pathway [63]. ALP conjugated QDs have been linked to gold electrode to develop an electrochemical sensor for *p*-aminophenylphosphate [64]. AChE (EC 3.1.1.7) is a tetrameric enzyme which plays a critical role in acetylcholine-mediated neurotransmission [65]. It is an important target for several natural toxins, insecticides, nerve gases and diseases that involve compromised acetylcholine-mediated neurotransmission. AChE conjugated CdS nanoparticles have been previously employed as a photo-electrochemical label for sensing chemical warfare agents which act as inhibitors of AChE [66]. There have been earlier reports where recombinant human butyrylcholinesterase has been conjugated to QD by adsorption and shown adhering to membrane of live cells [32].

2. Experimental

2.1. Materials

Hen egg white lysozyme (HEWL) (L-6876), freeze-dried cells of *Micrococcus lysodeikticus* (A.T.C.C. 4698), acrylamide, N,N′-methylene-bisacrylamide, N,N,N′,N′-tetramethylethylenediamine (TEMED), alkaline phosphatase (P7640, bovine intestinal mucosa) and acetylcholinesterase (C3389, *Electrophorus electricus*, electric eel) were procured from Sigma-Aldrich Chemicals Pvt. Ltd., New Delhi. The enzymes were used without further purification. 2-Naphthyl acetate was purchased from Fluka. Sodium dihydrogen phosphate (NaH_2PO_4), glycine, disodium hydrogen phosphate (Na_2HPO_4), sodium bicarbonate ($NaHCO_3$), sodium dodecyl sulfate (SDS), dimethyl formamide (DMF) HPLC grade, and ammonium persulfate (APS) were obtained from Merck Limited (Worli, Mumbai), and p-nitrophenyl phosphate disodium salt (PNPP) was bought from Sisco Research Laboratories, India. Streptavidin conjugated quantum dots (Qdot® 525, Q10141 MP or Q10041 MP) and protein biotinylation reagents (DSB-X™ kit, D-20655) were procured from Invitrogen, USA. All other chemicals employed were of analytical grade.

2.2. Methods

2.2.1. Initial rate kinetics of enzymes

The catalytic activities of all enzymes were measured at 298 K using a Varian Cary 100 UV–visible spectrophotometer employing double beam optics. Changes in absorbance owing to enzyme reaction were acquired at 1 second intervals for a period ranging from 600 s to 40 min depending on the enzyme studied. The data for initial 20–30 s during which the change in absorbance was a linear function of time was used to calculate the initial rate. All samples were made in deionized water. The initial velocities observed under identical conditions were measured in triplicates on different days to account for experimental errors. Blank solution consisted of only substrates which showed a negligible change in the absorbance in the complete absence of enzyme under identical conditions, proving that substrates and other agents were chemically inert throughout the reaction time. The saturation kinetics was carried out multiple times for all enzymes and the values of V_{max} and K_m obtained were averaged for use in further experiments. The initial rates obtained from a series of substrate concentrations were fitted using nonlinear least square regression to a Michaelis–Menten equation for obtaining V_{max} and K_m values. The enzyme activity was measured for the three different substrate concentrations (0.5 K_m, K_m and 3 K_m) corresponding to half saturation constant (K_m). HEWL activity was determined at 298 K by measuring the rate of decrease (slope for the first 30 s) in absorbance (proportional to sample turbidity) at 450 nm. A stock solution of *M. lysodeikticus* (5 mg/mL) was freshly prepared in water and diluted finally to various concentrations ranging from 10 μg/mL to 500 μg/mL in assay buffer (150 mM phosphate buffer, pH 7, ionic strength 0.15). The K_m of HEWL for *M. lysodeikticus* was determined to be 150 μg/mL (Supplementary Fig. S1).

Similarly, the kinetic parameters of ALP were determined at 298 K by measuring the rate of increase (slope for the first 30 s) in the absorbance at 405 nm due to hydrolysis of p-nitrophenyl phosphate disodium salt (PNPP) employed as substrate at pH 9. The K_m of alkaline phosphatase for PNPP was determined as 60 μM (Supplementary Fig. S2).

Lastly AChE activity was determined at 298 K by measuring the rate of increase (slope for the first 20 s) in the absorbance of the solution at 320 nm due to the formation of 2-naphthol from the hydrolysis of 2-naphthyl acetate employed as substrate at pH 7.5. The K_m of AChE for 2-naphthyl acetate was determined as 727 μM (Supplementary Fig. S3).

2.2.2. Biotinylation of enzymes and their conjugation to QDs

Enzyme biotinylation with a DSB-X™ biotin protein labeling kit was carried out following protocol given by the supplier. The kit includes amine-reactive DSB-X biotin succinimidyl ester that incorporates a seven-atom spacer to increase the ability of the DSB-X biotin moiety to bind in the deep biotin-binding pocket of streptavidin [67,68]. Unbound biotin was removed by dialysis. Since this method randomly biotinylates the exposed lysine residues, the stoichiometric ratio of biotin reactive agent/protein was varied between 0 and 4, so as to assess the effect of increasing level of biotinylation on the catalytic activity of enzymes before their conjugation to streptavidin coated QDs. The

biotinylated proteins were incubated with the required amount of streptavidin coated QDs, present in a 1 μM stock solution. As per information from the vendor each QD contains about 5–10 streptavidins attached on its surface making the overall diameter of the conjugate at 15–20 nm. Since each streptavidin has three available sites (one site occupied in the bond with the QD), there were a total of 15–30 protein binding sites on each QD. The concentrations of QDs calculated as per the above population of protein binding sites were taken in slight excess to avoid the presence of any unconjugated biotinylated enzyme which could complicate kinetics. Streptavidin coated QDs were incubated with biotinylated enzymes under mild stirring conditions for 2 h at 298 K.

2.3. Characterization of QD–Enz conjugates

2.3.1. Luminescence spectrometry

All luminescence studies were performed on a FluoroMax-3 steady-state spectrofluorometer purchased from Jobin Yvon Inc., USA. The consequence of conjugating enzyme to the QD was studied by measuring the luminescence from QD. The QD emission spectra were acquired in response to excitation at 420 nm in separate experiments. The excitation and emission slit widths were kept at 1 and 3 nm, respectively. As excitation at 280 nm leads to excitation of both QD and tryptophan in protein, the excitation at 420 nm was chosen as it solely excites the QD component in the conjugate. The stability of unconjugated QDs and QD–Enz conjugates in aqueous buffers corresponding to the chosen enzyme reaction was monitored by recording luminescence over a period of 3 days.

2.3.2. Gel electrophoresis

To ascertain the conjugation of QD with enzyme, non-denaturing polyacrylamide gel electrophoresis was done. Due to poor resolution of the bands in PAGE (not shown), agarose gel electrophoresis was done. Although HEWL is positively charged at pH 7 (TAE buffer, pI ~ 11.3), when conjugated to QDs, the latter's charge becomes highly dominant. SDS had to be added to impart an overall negative charge to HEWL samples. ALP and AChE have isoelectric points less than 7 and thus are expected to be negatively charged. Also QDs moved towards the positive electrode as expected.

3. Results and discussion

3.1. Catalytic activity of QDEnzBio conjugates

For assessing the catalytic activity of the hydrolytic enzymes, the initial rate kinetics with appropriate substrates was measured. These measurements were performed before biotinylation (control), after biotinylation and post conjugation of enzyme to QDs.

3.1.1. Hen egg white lysozyme (HEWL)

HEWL activity was measured by monitoring the lysis of *M. lysodeikticus* cells [69]. Firstly, the effect of biotinylation on the HEWL activity was probed. Fig. 1A shows that an increasing level of biotinylation (as quantified by biotin/HEWL stoichiometric ratio) led to a gradual drop in the initial rate of hydrolysis by biotinylated HEWL for all substrate concentrations. Interestingly while the drop varied linearly with increased biotin for higher substrate concentrations (K_m and 3 K_m), it revealed a quadratic dependence with lowest substrate concentration (0.5 K_m). A linear dependence reflects loss of active enzyme population with biotinylation while a complex saturation behavior hints at insensitivity of the enzyme in the presence of low substrate levels with increased biotinylation. Thus, increased biotinylation in HEWL leads to a corresponding decrease in HEWL enzymatic activity. The reaction kinetics profile of HEWL–QD conjugates is depicted in Fig. 1B. It is noted that absolute values of the rates reveal almost no change implying that conjugation with QD has negligible influence on

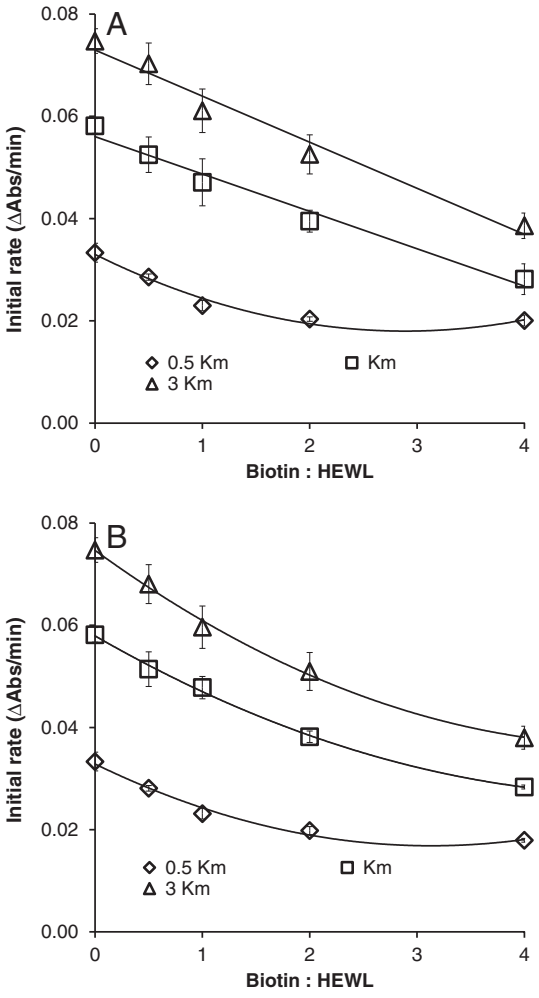

Fig. 1. HEWL activity after biotinylation and after conjugation to QDs. (A) The initial rate of hydrolysis in *M. lysodeikticus* suspension catalyzed by 136 nM HEWL is plotted against the extent of biotinylation in the HEWL employed for the reaction in the absence of quantum dots. (B) The initial rate of hydrolysis in *M. lysodeikticus* suspension catalyzed by 136 nM HEWL is plotted against the extent of biotinylation in the HEWL employed for the reaction in the presence of streptavidin coated quantum dots (7 nM). The plots are shown for the three different substrate concentrations (0.5 K_m represented by diamonds, K_m represented by squares and 3 K_m represented by triangles). K_m and V_{max} values for HEWL under the conditions employed for the reactions above were determined as ~150 μg/mL and 0.073 ΔAbs/min, respectively (see Supplementary Fig. S1). Error bars indicate standard deviation, where n = 3.

HEWL kinetics. However the kinetics at all substrate concentrations reveal a declining quadratic dependence with the extent of HEWL biotinylation unlike the linear dependence observed in the absence of QD. The full time courses of HEWL catalyzed hydrolysis for results presented in Fig. 1 are shown in Supplementary Fig. S4.

The marked decrease in activity of HEWL with the degree of biotinylation needed further investigation. Increasing the ionic strength of the reaction buffer is known to have profound effects on HEWL activity over the pH range 6.2–9.0 [61]. Since HEWL (pI ~ 11.3) was positively charged in the pH range employed, while the bacterial cell membranes (substrate) were negatively charged, electrostatic interactions played a major role in facilitating the binding of HEWL active site to bacterial cell wall surface. As pH was raised maintaining a constant but high ionic strength, the net positive charge on HEWL diminished resulting in weaker electrostatic interactions with bacterial substrate, contributing to catalytic inhibition [61]. Therefore, it would be safe to assume that the ionic strength used in our reaction might have been high enough to cause the observed decline in enzyme activity in Fig. 1. To verify this, the enzymatic reaction of biotinylated HEWL was carried out in

the presence of varying ionic strengths (50–150 mM NaCl) under two different substrate concentrations (0.5 K_m and 3 K_m) as shown in Fig. 2A and B. It is evident that increasing ionic strength in the reaction medium causes a more pronounced decline in enzyme activity with increasing biotinylation. This decline is further magnified at higher substrate concentrations. The high ionic strength probably screens out the electrostatic attraction between negatively charged substrate and positively charged HEWL surface that is critical for the enzymatic reaction.

The decline in HEWL activity even at low ionic strength is intriguing. The biotinylation of exposed lysine residues on the HEWL surface (Supplementary Fig. S10) probably eliminates the positive charge in the ε-amino group thereby reducing the net charge on the protein. Therefore increased biotinylation may diminish the positive charge on HEWL akin to raising pH as discussed above. It is thus likely that the combined effect of overall reduced charge due to biotinylation of lysine and screening of the charges by high ionic strength probably weakens the electrostatic interaction between HEWL and bacterial cell membrane causing a drop in activity. In addition, there is a possibility of disruption in local structure among the α-helices which stabilize the active site. As three of the six accessible lysine residues for biotinylation are intrinsic to the five different α-helices any charge reduction (in this case, biotinylation) may disrupt existing salt bridges affecting the overall tertiary structure and consequently substrate binding.

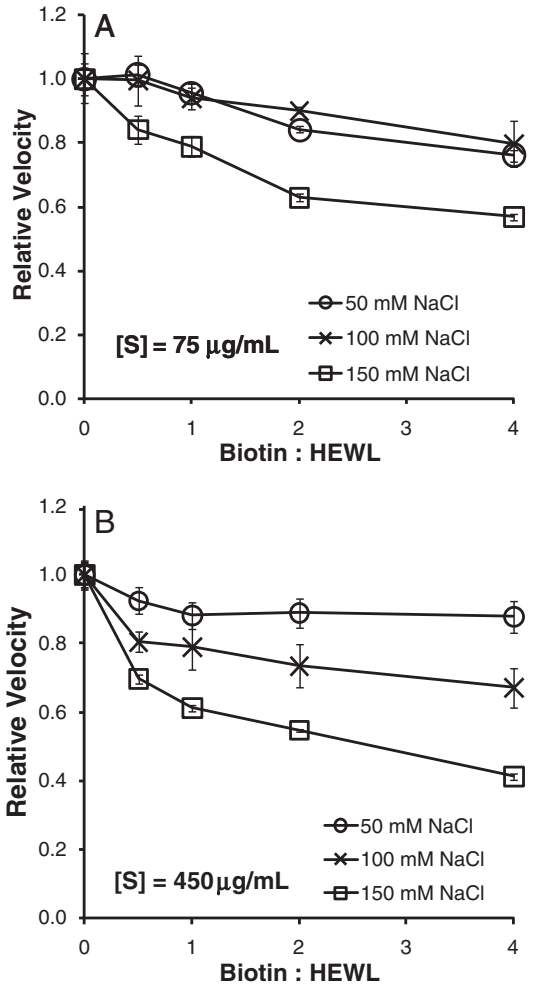

Fig. 2. The effect of ionic strength on catalytic rate of biotinylated HEWL. The decrease in the rate of hydrolysis in *M. lysodeikticus* suspension by biotinylated HEWL is displayed against the extent of HEWL biotinylation for different concentrations of NaCl in the medium. Panel A depicts the effects observed at low substrate (75 µg/mL), while panel B shows the same at high substrate (450 µg/mL). Note the significant dip in activity as ionic strength increases. Error bars indicate standard deviation, where n = 3.

3.1.2. Alkaline phosphatase (ALP)

The effect of biotinylation of ALP on its catalytic rate was measured and no significant variation in the rate of hydrolysis was observed with an increase in biotinylation of ALP (Fig. 3A). Fig. 3B displays a similar plot subsequent to incubation with ALP–QD conjugates. Here too, no noteworthy changes were observed on the rate of PNPP hydrolysis as a function of ALP biotinylation. The full time course of ALP catalyzed hydrolysis for the results presented in Fig. 3 is shown in Supplementary Fig. S5. These results clearly demonstrate that biotinylating and conjugating ALP to QDs has negligible impact on its hydrolytic enzymatic rate. Thus, there is little disruption of substrate binding and active site environment of ALP during catalysis owing to biotinylation and conjugation to QD.

A major factor that could account for the activity retention in ALP is the predominant presence of lysine groups in loops and turns in the enzyme structure unlike HEWL where they reside in alpha helices (Supplementary Fig. S10A, B). Another plausible cause might be the large number of lysine groups in the ALP polypeptide chain that appear distant from active site in comparison to HEWL, such that loss of few

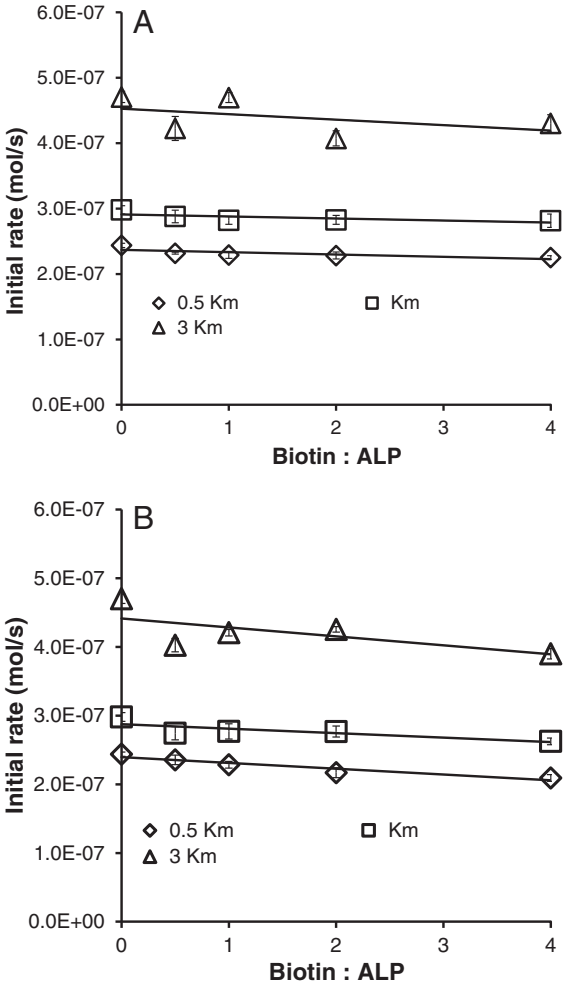

Fig. 3. ALP activity after biotinylation and after conjugation to QDs. (A) The initial rate of p-nitrophenyl phosphate hydrolysis catalyzed by 250 nM ALP is plotted against extent of biotinylation in the ALP employed for the reaction in the absence of quantum dots. (B) The initial rate of p-nitrophenyl phosphate hydrolysis catalyzed by 250 nM ALP is plotted against the extent of biotinylation in the ALP employed for the reaction in the presence of streptavidin coated quantum dots (10 nM). The plots are shown for the three different substrate concentrations as mentioned in Fig. 1. K_m and V_{max} values for ALP under the conditions employed for the reactions above were determined as ~60 µM and 6.7×10^{-7} mol·s^{-1}, respectively (see Supplementary Fig. S2). Error bars indicate standard deviation, where n = 3.

positive charges due to lysine biotinylation may not alter protein conformation.

3.1.3. Acetylcholinesterase (AChE)

The effect of AChE biotinylation on its catalytic rate is shown in Fig. 4A for different concentrations of 2-naphthyl acetate. A marginal dip in the rate of hydrolysis was observed at highest substrate concentration (3 K_m), while for lower substrate concentrations no significant variation in the rate of hydrolysis with increase in biotinylation of AChE was detectable. Fig. 4B displays a similar plot of catalytic rate of AChE–QD conjugates. Here no significant changes were observed in the catalytic rate of for all substrate concentrations. The full time course of AChE catalyzed hydrolysis for the results presented in Fig. 4 are shown in Supplementary Fig. S6. The reason for the robustness of AChE towards QD binding may be ascertained by the fact that the catalytic domain of AChE is situated in a 20 Å deep gorge (Supplementary Fig. S10C) away from the amino acid residues on the surface, thus it remains unaffected by the QD binding. The gorge itself along with amino acid residues in its vicinity are devoid of lysine residues, thereby avoiding the possibility of biotin attaching at the entry or neighborhood of the gorge. Hence it appears unlikely for a QD to pose steric hindrance for substrate molecules entering the gorge.

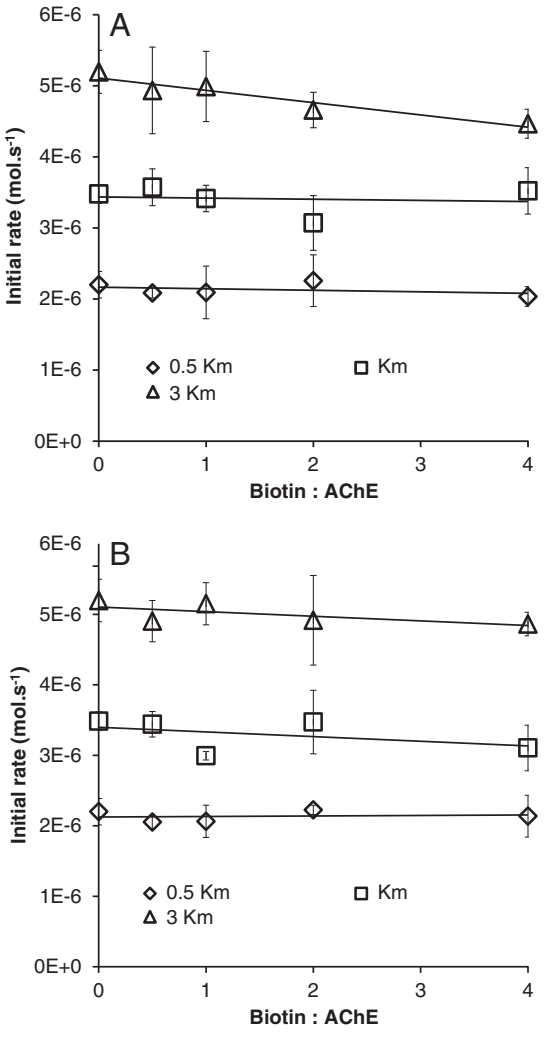

Fig. 4. AChE activity after biotinylation and after conjugation to QDs. (A) The initial rate of 2-naphthyl acetate hydrolysis catalyzed by 21.6 nM AChE is plotted against the extent of biotinylation in the AChE employed for the reaction in the absence of quantum dots. (B) The initial rate of 2-naphthyl acetate hydrolysis catalyzed by 21.6 nM AChE is plotted against the extent of biotinylation in the AChE employed for the reaction in the presence of streptavidin coated quantum dots (1.0 nM). The plots are shown for the three different substrate concentrations as mentioned in Fig. 1. K_m and V_{max} values for AChE under the conditions employed for the reactions above were determined as ~727 μM and 1.07×10^{-5} mol·s^{-1}, respectively (see Supplementary Fig. S3). Error bars indicate standard deviation, where n = 3.

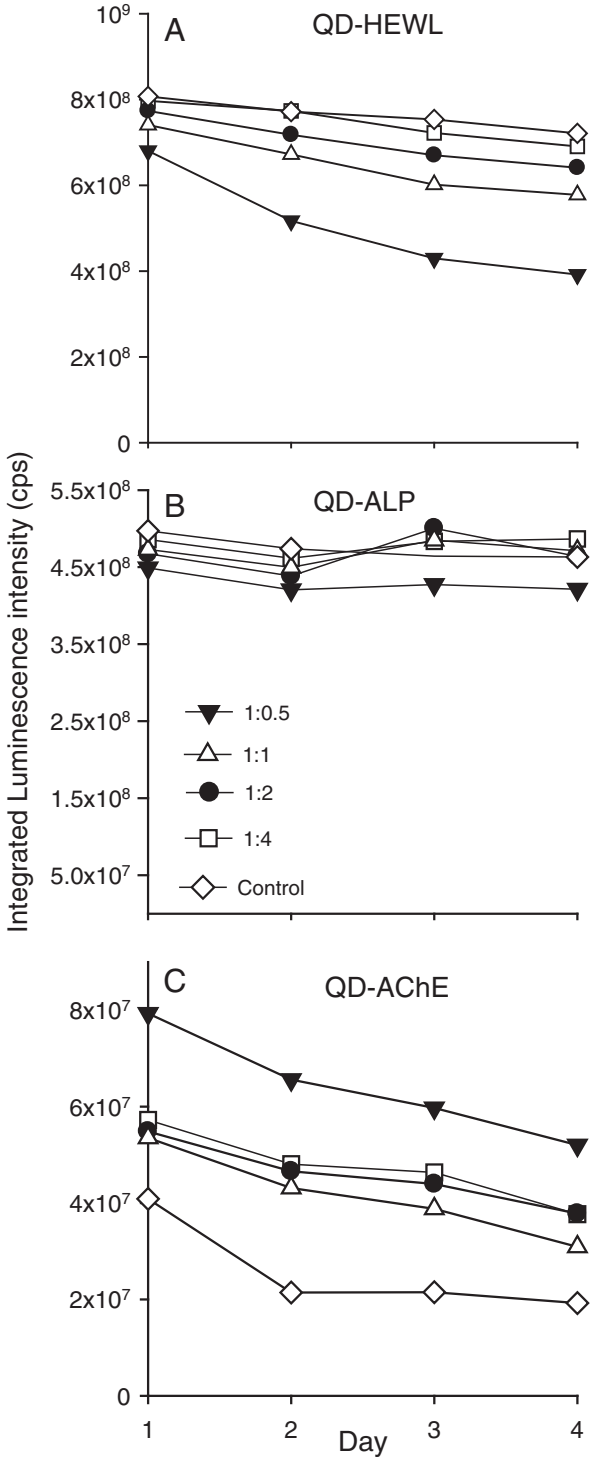

Fig. 5. Luminescence intensity of QD–Enz conjugates. The observed integrated luminescence intensity of QD–Enz conjugates incubated in different buffers and stored at 277 K is shown from day 1 (the day when conjugation was performed) to day 4. Control refers to QD alone in the absence of enzyme, while the remaining symbols indicate the enzyme:biotin stoichiometric ratio during biotinylation reaction. (A) QD–HEWL conjugates in pH 7.4 PBS buffer; (B) QD–ALP conjugates in pH 9 glycine buffer; and (C) QD—AChE conjugates in pH 7.5 phosphate buffer. The emission spectra used for calculating the luminescence yields (A), (B) and (C) are shown in Supplementary Figs. S7–S9, respectively.

In all QD–Enz conjugates above, the distance of enzyme from QD surface and its orientation on the QD surface appears appropriate, as all conjugates are fully functional. The distance has been optimized by vendor by choosing the length of the spacer between enzyme surface and biotin such that enzyme-linked biotin can access the three high affinity binding sites [70] ($K_d = 10^{-15}$ M) that are partially buried in every streptavidin molecule [39] linked to QD. Importantly in comparison to previous conjugation strategies listed in Table 1, the streptavidin–biotin chemistry appears to be promising and universally suitable for creating fully functional QD–Enz conjugates as demonstrated for the three enzymes here.

3.2. Luminescence of QD–Enz conjugates

To ascertain the robustness of QDs, their luminescence was monitored for three days post-conjugation to enzymes. The QD–Enzs were excited at 420 nm to avoid luminescence contribution from enzymes. Fig. 5 provides a comprehensive summary of the integrated luminescence yield obtained from different QD–Enz conjugates on each passing day post-conjugation.

In Fig. 5A, experiments using streptavidin coated QDs alone (*control*) revealed only a marginal drop in photoluminescence (PL) counts when stored in PBS buffers at pH 7.4 (see also Supplementary Fig. S7). However, in the presence of increasing levels of biotinylated-HEWL, we observe a sharp drop in intensity starting with 1:0.5 ratio but this decline gradually diminishes as biotin levels in HEWL rise. At the highest level (1:4), the decline in luminescence is nearly the same as that observed with control. Thus at maximal biotinylation, biotinylated-HEWL remains equally luminescent as control QD in PBS.

Fig. 5B presents a different scenario. Here, the control QDs reveal insignificant change in luminescence when incubated in pH 9.0 for 3 days (see also Supplementary Fig. S8). However, in the presence of biotinylated-ALP, while a marginal dip in luminescence is seen with low biotinylation (1:0.5), higher biotin ratios show luminescence yields nearly equal and occasionally higher than control during incubation. Thus biotinylated-ALP too remains equally luminescent as control QD at pH 9.

In Fig. 5C, it is seen that in pH 7.5 buffer, the luminescence from control QDs is significantly reduced on day 2 and consistently remains so later (see also Supplementary Fig. S9). However in the presence of biotinylated-AChE, a two-fold rise in QD luminescence is observed at low biotin ratio (1:0.5) over control QDs. Although this increase is noticeably reduced as levels of biotinylation in AChE increase, the QD luminescence in the presence of biotinylated-AChE still remains significantly high in comparison to control QDs. Thus biotinylated-AChE is more luminescent compared to control QD at pH 7.5.

Interestingly, there was no measurable shift observed in the peak emission wavelength at ~525 nm (Supplementary Figs. S7–S9). This indicates that there was no aggregation amongst the QDs after 3 days of incubation in aqueous buffers [71]. Together with the fact that luminescence intensity from QD is conserved among all QD–Enz conjugates, this suggests that structurally the QDs were intact at all the conditions employed.

The loss of QD luminescence intensity among the control samples can arise from ionic attacks in aqueous solutions as reported elsewhere [24]. Previous reports have indicated that in physiological buffers: ionic attacks, time dependent increase in the dark dot population and occasional precipitation in aqueous buffers contributes to the loss of QD luminescence. Spontaneous formation of protein corona around the QD sphere prevents this loss by restricting access to ions in the solution and modifying their surface charge states [72]. This is clearly evident here in the case of AChE–QD conjugates (Fig. 5C) where increased biotinylation in AChE enhances luminescence. The diminished luminescence observed with low biotinylation ratios in Fig. 5A and B might arise from non-specific binding of non-biotinylated HEWL or ALP to QD surface, leading to quenching. This quenching is clearly abolished when strongly specific biotin–avidin interactions take over at high biotinylation ratios (Fig. 5). Thus increased biotinylation of the enzyme guarantees that enzyme shall be conjugated to the streptavidin coated QD and not directly adsorbed on the QD surface. The data in Fig. 5 thus prove that the enzymes have indeed been biotinylated and conjugated to QDs.

3.3. Agarose gel electrophoresis

To further ascertain that QDs have indeed been conjugated to enzymes, agarose gel electrophoresis of the QD–Enz conjugates was performed as shown in Fig. 6. The results of agarose gel electrophoresis for different QD–Enz conjugates clearly reveal slowed migration of QD–Enz conjugates in comparison to QDs alone. The extent to which QD–Enz conjugates are slowed down in comparison to pure QDs increases in the order HEWL < ALP < AChE which is in line with their increasing molecular weights. This confirms that all biotinylated enzymes are indeed bound to QDs and the corresponding catalytic activities arise from such conjugates only. As there are 15–30 streptavidins per QD (as per vendor), it is likely that no more than 30 enzyme molecules are

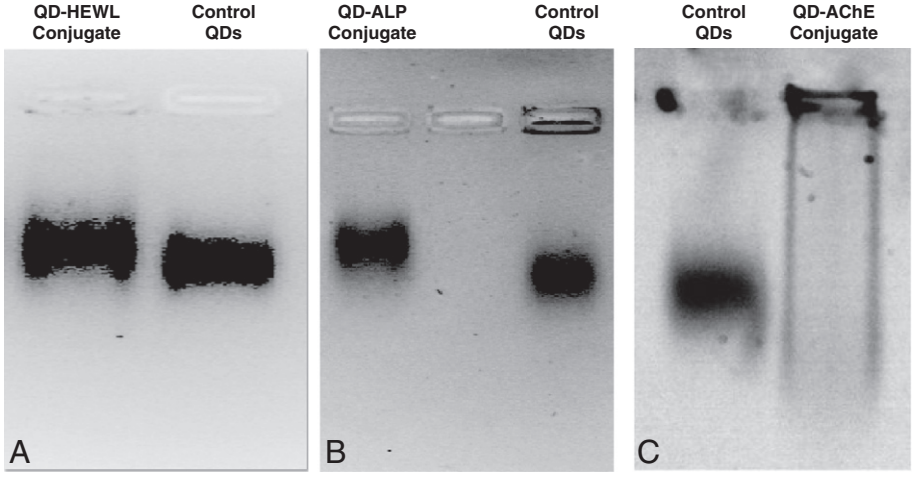

Fig. 6. Agarose gel electrophoresis of QD–Enz conjugates. The electrophoretic mobility of QDs alone (control) and QD–Enz conjugates in agarose gel is depicted as follows: (A) control and QD–HEWL in 1.5% agarose gel; (B) control and QD–ALP in 1.5% agarose gel; (C) control and QD–AChE in 0.4% agarose gel. For (A) and (B) 500 nM of QDs was loaded in the gel, while for (C) 1 nM was loaded. The gel was run at constant voltage conditions for approximately 3 h. All images have been contrasted equally for emphasis of differences in migration rates.

conjugated to each QD. However, this number is probably far less for bulky enzymes like AChE compared to HEWL owing to surface crowding and steric effects.

The dark luminescence bands in the agarose gel reflect the high extinction coefficient and luminescence quantum yield of QDs on exposure to ultraviolet wavelengths. The poor separation between bands in Fig. 6A and B is not a surprise with QDs on gel electrophoresis as previous reports indicate [71,73,74]. QDs are large molecules with molecular weights near ~400 kDa. In addition, each streptavidin molecule is around 75 kDa [75], which gives a total molecular weight to be around ~925 kDa (considering an average of 7 streptavidin molecules per QD). This large molecular weight of QD in comparison to enzymes (14–280 kDa) probably accounts for the poor separation between bands observed in the gels. The negligible movement of AChE–QD conjugates is accounted by large size of tetrameric enzyme (~280 kDa), making QD–Enz conjugates too large for entry into the pores of the agarose gel.

Although we have not measured the exact number of enzymes conjugated to QD surface, increased level of enzyme biotinylation raises the packing density of enzymes in QD surface as confirmed by QD luminescence data. Hence, the observation of complete enzyme activity in QDEnzBio with bulky macromolecules like AChE and ALP (Figs. 3 and 4) at all biotinylation levels indicates that the packing density of enzymes on QD surface is moderate enough to permit enzyme to retain native-like activity. Higher packing densities may be needed to start observing decline in enzyme activity brought about by crowded QD surface.

4. Conclusions

In this study, the effect of biotinylation and conjugation of hydrolytic enzymes HEWL, ALP and AChE to QDs was investigated. All three enzymes revealed a negligible change in their catalytic activity upon conjugation to QDs *via* streptavidin–biotin linkage. In the case of biotinylated HEWL, the enzyme activity was profoundly affected by degree of biotinylation and salt concentration in the medium but this was irrespective of conjugation to the QD. The stability (luminescence) of QDs was preserved in all QD–Enz conjugates. Thus, we conclude that the streptavidin–biotin chemistry is universally best suited for engineering functional and luminescent QD–Enz conjugates in comparison to other existing approaches.

Acknowledgements

We thank Prof. Vinod Subramaniam from FOM Institute AMOLF for his comments on the manuscript. RS acknowledges the funding from Council for Scientific and Industrial Research, New Delhi under Ref: 37/1373/09 EMR II that made this work possible.

Appendix A. Supplementary data

The Michaelis–Menten kinetics of HEWL (Figure S1), ALP (S2) and AChE (S3); absorbance *vs.* time traces of HEWL(S4), ALP(S5) and AChE(S6) catalyzed hydrolysis reactions; emission spectra of QD-HEWL(S7), QD-ALP(S8) and QD-AChE(S9) conjugates and structure of enzymes investigated in this study(S10) are displayed here.

Supplementary data to this article can be found online at http://dx.doi.org/10.1016/j.bbagen.2014.06.003.

References

[1] U. Resch-Genger, M. Grabolle, S. Cavaliere-Jaricot, R. Nitschke, T. Nann, Quantum dots versus organic dyes as fluorescent labels, Nat. Methods 5 (2008) 763–775.
[2] Z. Ning, D. Zhitomirsky, V. Adinolfi, B. Sutherland, J. Xu, O. Voznyy, P. Maraghechi, X. Lan, S. Hoogland, Y. Ren, E.H. Sargent, Graded doping for enhanced colloidal quantum dot photovoltaics, Adv. Mater. 25 (2013) 1719–1723.
[3] J. Tang, K.W. Kemp, S. Hoogland, K.S. Jeong, H. Liu, L. Levina, M. Furukawa, X. Wang, R. Debnath, D. Cha, K.W. Chou, A. Fischer, A. Amassian, J.B. Asbury, E.H. Sargent, Colloidal-quantum-dot photovoltaics using atomic-ligand passivation, Nat. Mater. 10 (2011) 765–771.
[4] J.C. Claussen, N. Hildebrandt, K. Susumu, M.G. Ancona, I.L. Medintz, Complex logic functions implemented with quantum dot bionanophotonic circuits, ACS Appl. Mater. Interfaces 6 (2014) 3771–3778.
[5] J.C. Claussen, W.R. Algar, N. Hildebrandt, K. Susumu, M.G. Ancona, I.L. Medintz, Biophotonic logic devices based on quantum dots and temporally-staggered Forster energy transfer relays, Nanoscale 5 (2013) 12156–12170.
[6] M. Esposito, N. Kumar, K. Lindenberg, C. Van den Broeck, Stochastically driven single-level quantum dot: a nanoscale finite-time thermodynamic machine and its various operational modes, Phys. Rev. E. 85 (2012) 031117.
[7] D. Venturelli, R. Fazio, V. Giovannetti, Minimal self-contained quantum refrigeration machine based on four quantum dots, Phys. Rev. Lett. 110 (2013) 256801.
[8] Y. Shi, Y. Pan, H. Zhang, Z. Zhang, M.J. Li, C. Yi, M. Yang, A dual-mode nanosensor based on carbon quantum dots and gold nanoparticles for discriminative detection of glutathione in human plasma, Biosens. Bioelectron. 56 (2014) 39–45.
[9] H. Liu, M. Li, O. Voznyy, L. Hu, Q. Fu, D. Zhou, Z. Xia, E.H. Sargent, J. Tang, Physically flexible, rapid-response gas sensor based on colloidal quantum dot solids, Adv. Mater. 26 (2014) 2718–2724.
[10] B. The Huy, M.H. Seo, X. Zhang, Y.I. Lee, Selective optosensing of clenbuterol and melamine using molecularly imprinted polymer-capped CdTe quantum dots, Biosens. Bioelectron. 57 (2014) 310–316.
[11] Y. Shirasaki, G.J. Supran, M.G. Bawendi, V. Bulović, Emergence of colloidal quantum-dot light-emitting technologies, Nat. Photonics 7 (2013) 13–23.
[12] W. Mu, P. Zhang, J. Xu, S. Sun, J. Xu, W. Li, K. Chen, Direct-current and alternating-current driving Si quantum dots-based light emitting device, IEEE J. Sel. Top. Quantum Electron. 20 (2014) 8200106.
[13] X. Michalet, F.F. Pinaud, L.A. Bentolila, J.M. Tsay, S. Doose, J.J. Li, G. Sundaresan, A.M. Wu, S.S. Gambhir, S. Weiss, Quantum dots for live cells, in vivo imaging, and diagnostics, Science 307 (2005) 538–544.
[14] H. Tada, H. Higuchi, T.M. Wanatabe, N. Ohuchi, In vivo real-time tracking of single quantum dots conjugated with monoclonal anti-HER2 antibody in tumors of mice, Cancer Res. 67 (2007) 1138–1144.
[15] F. Duconge, T. Pons, C. Pestourie, L. Herin, B. Theze, K. Gombert, B. Mahler, F. Hinnen, B. Kuhnast, F. Dolle, B. Dubertret, B. Tavitian, Fluorine-18-labeled phospholipid quantum dot micelles for in vivo multimodal imaging from whole body to cellular scales, Bioconjug. Chem. 19 (2008) 1921–1926.
[16] T. Ohyanagi, N. Nagahori, K. Shimawaki, H. Hinou, T. Yamashita, A. Sasaki, T. Jin, T. Iwanaga, M. Kinjo, S. Nishimura, Importance of sialic acid residues illuminated by live animal imaging using phosphorylcholine self-assembled monolayer-coated quantum dots, J. Am. Chem. Soc. 133 (2011) 12507–12517.
[17] A.P. Alivisatos, W. Gu, C. Larabell, Quantum dots as cellular probes, Annu. Rev. Biomed. Eng. 7 (2005) 55–76.
[18] T.V. Torchynska, Emission of double core infrared (CdSeTe)/ZnS quantum dots conjugated to antibodies, J. Lumin. 137 (2013) 157–161.
[19] S. Kwon, Single-molecule fluorescence in situ hybridization: quantitative imaging of single RNA molecules, BMB Rep. 46 (2013) 65–72.
[20] I.L. Medintz, H.T. Uyeda, E.R. Goldman, H. Mattoussi, Quantum dot bioconjugates for imaging, labelling and sensing, Nat. Mater. 4 (2005) 435–446.
[21] L. Cao, J. Ye, L. Tong, B. Tang, A new route to the considerable enhancement of glucose oxidase (GOx) activity: the simple assembly of a complex from CdTe quantum dots and GOx, and its glucose sensing, Chem. Eur. J. 14 (2008) 9633–9640.
[22] Q. Liu, X. Lu, J. Li, X. Yao, J. Li, Direct electrochemistry of glucose oxidase and electrochemical biosensing of glucose on quantum dots/carbon nanotubes electrodes, Biosens. Bioelectron. 22 (2007) 3203–3209.
[23] P. Wu, Y. He, H.F. Wang, X.P. Yan, Conjugation of glucose oxidase onto Mn-doped ZnS quantum dots for phosphorescent sensing of glucose in biological fluids, Anal. Chem. 82 (2010) 1427–1433.
[24] C.P. Huang, Y.K. Li, T.M. Chen, A highly sensitive system for urea detection by using CdSe/ZnS core-shell quantum dots, Biosens. Bioelectron. 22 (2007) 1835–1838.
[25] U.S. Akshath, L.R. Shubha, P. Bhatt, M.S. Thakur, Quantum dots as optical labels for ultrasensitive detection of polyphenols, Biosens. Bioelectron. 57 (2014) 317–323.
[26] J. Yuan, W. Guo, E. Wang, Utilizing a CdTe quantum dots–enzyme hybrid system for the determination of both phenolic compounds and hydrogen peroxide, Anal. Chem. 80 (2008) 1141–1145.
[27] E.R. Goldman, A.R. Clapp, G.P. Anderson, H.T. Uyeda, J.M. Mauro, I.L. Medintz, H. Mattoussi, Multiplexed toxin analysis using four colors of quantum dot fluororeagents, Anal. Chem. 76 (2004) 684–688.
[28] J.H. Kim, S. Chaudhary, M. Ozkan, Multicolour hybrid nanoprobes of molecular beacon conjugated quantum dots: FRET and gel electrophoresis assisted target DNA detection, Nanotechnology 18 (2007) 195105.
[29] R. Freeman, Y. Li, R. Tel-Vered, E. Sharon, J. Elbaz, I. Willner, Self-assembly of supramolecular aptamer structures for optical or electrochemical sensing, Analyst 134 (2009) 653–656.
[30] R. Freeman, T. Finder, R. Gill, I. Willner, Probing protein kinase (CK2) and alkaline phosphatase with CdSe/ZnS quantum dots, Nano Lett. 10 (2010) 2192–2196.
[31] V. Bagalkot, L. Zhang, E. Levy-Nissenbaum, S. Jon, P.W. Kantoff, R. Langery, O.C. Farokhzad, Quantum dot–aptamer conjugates for synchronous cancer imaging, therapy, and sensing of drug delivery based on Bi-fluorescence resonance energy transfer, Nano Lett. 7 (2007) 3065–3070.
[32] N. Waiskopf, I. Shweky, I. Lieberman, U. Banin, H. Soreq, Quantum dot labeling of butyrylcholinesterase maintains substrate and inhibitor interactions and cell adherence features, ACS Chem. Neurosci. 2 (2011) 141–150.
[33] R. Sarkar, S.S. Narayanan, L.O. Pålsson, F. Dias, A. Monkman, S.K. Pal, Direct conjugation of semiconductor nanocrystals to a globular protein to study protein-folding intermediates, J. Phys. Chem. B 111 (2007) 12294–12298.

[34] W.R. Algar, D.E. Prasuhn, M.H. Stewart, T.L. Jennings, J.B. Blanco-Canosa, P.E. Dawson, I.L. Medintz, The controlled display of biomolecules on nanoparticles: a challenge suited to bioorthogonal chemistry, Bioconjug. Chem. 22 (2011) 825–858.
[35] M.E. Aubin-Tam, K. Hamad-Schifferli, Structure and function of nanoparticle–protein conjugates, Biomed. Mater. 3 (2008) 034001.
[36] K.E. Sapsford, W.R. Algar, L. Berti, K.B. Gemmill, B.J. Casey, E. Oh, M.H. Stewart, I.L. Medintz, Functionalizing nanoparticles with biological molecules: developing chemistries that facilitate nanotechnology, Chem. Rev. 113 (2013) 1904–2074.
[37] J.B. Blanco-Canosa, M. Wu, K. Susumu, E. Petryayeva, T.L. Jennings, P.E. Dawson, W.R. Algar, I.L. Medintz, Recent progress in the bioconjugation of quantum dots, Coord. Chem. Rev. 263–264 (2014) 101–137.
[38] J. Wang, Y. Nie, Y. Lu, J. Liu, J. Wang, A. Fu, T. Liu, J. Xia, Assembly of multivalent protein ligands and quantum dots: a multifaceted investigation, Langmuir 30 (2014) 2161–2169.
[39] M. Li, K.K.W. Wong, S. Mann, Organization of inorganic nanoparticles using biotin–streptavidin connectors, Chem. Mater. 11 (1999) 23–26.
[40] R. Bardhan, W. Chen, M. Bartels, C. Perez-Torres, M.F. Botero, R.W. McAninch, A. Contreras, R. Schiff, R.G. Pautler, N.J. Halas, A. Joshi, Tracking of multimodal therapeutic nanocomplexes targeting breast cancer in vivo, Nano Lett. 10 (2010) 4920–4928.
[41] C. Tekle, B. Van Deurs, K. Sandvig, T.G. Iversen, Cellular trafficking of quantum dot-ligand bioconjugates and their induction of changes in normal routing of unconjugated ligands, Nano Lett. 8 (2008) 1858–1865.
[42] M. Pulkkinen, J. Pikkarainen, T. Wirth, T. Tarvainen, V. Haapa-aho, H. Korhonen, J. Seppälä, K. Järvinen, Three-step tumor targeting of paclitaxel using biotinylated PLA–PEG nanoparticles and avidin–biotin technology: formulation development and in vitro anticancer activity, Eur. J. Pharm. Biopharm. 70 (2008) 66–74.
[43] J. Yuan, N. Gaponik, A. Eychmuller, Application of polymer quantum dot-enzyme hybrids in the biosensor development and test paper fabrication, Anal. Chem. 84 (2012) 5047–5052.
[44] C.C. Yu, Y.Y. Kuo, C.F. Liang, W.T. Chien, H.T. Wu, T.C. Chang, F.D. Jan, C.C. Lin, Site-specific immobilization of enzymes on magnetic nanoparticles and their use in organic synthesis, Bioconjug. Chem. 23 (2012) 714–724.
[45] Y. Song, D. Luo, S. Ye, M. Huang, D. Zhong, Z. Huang, H. Hou, L. Wang, Spectroscopic studies on the interaction between EcoRI and CdS QDs and conformation of EcoRI in EcoRI–CdS QDs bioconjugates, Phys. Chem. Chem. Phys. 14 (2012) 16258–16266.
[46] P.K. Verma, A. Giri, N.T.K. Thanh, L. Tung, O. Mondal, M. Pal, S.K. Pal, Superparamagnetic fluorescent nickel–enzyme nanobioconjugates: synthesis and characterization of a novel multifunctional biological probe, J. Mater. Chem. 20 (2010) 3722–3728.
[47] C.C. Yu, P.C. Lin, C.C. Lin, Site-specific immobilization of CMP-sialic acid synthetase on magnetic nanoparticles and its use in the synthesis of CMP-sialic acid, Chem. Commun. (2008) 1308–1310.
[48] A. Gole, C.J. Murphy, Azide-derivatized gold nanorods: functional materials for "click" chemistry, Langmuir 24 (2008) 266–272.
[49] S.S. Narayanan, R. Sarkar, S.K. Pal, Structural and functional characterization of enzyme–quantum dot conjugates: covalent attachment of CdS nanocrystal to alpha-chymotrypsin, J. Phys. Chem. C 111 (2007) 11539–11543.
[50] J.L. Brennan, N.S. Hatzakis, T.R. Tshikhudo, N. Dirvianskyte, V. Razumas, S. Patkar, J. Vind, A. Svendsen, R.J. Nolte, A.E. Rowan, M. Brust, Bionanoconjugation via click chemistry: the creation of functional hybrids of lipases and gold nanoparticles, Bioconjug. Chem. 17 (2006) 1373–1375.
[51] B.I. Ipe, C.M. Niemeyer, Nanohybrids composed of quantum dots and cytochrome P450 as photocatalysts, Angew. Chem. Int. Ed. Engl. 45 (2006) 504–507.
[52] M.E. Aubin, D.G. Morales, K. Hamad-Schifferli, Labeling ribonuclease S with a 3 nm Au nanoparticle by two-step assembly, Nano Lett. 5 (2005) 519–522.
[53] A. Gole, C. Dash, V. Ramakrishnan, S.R. Sainkar, A.B. Mandale, M. Rao, M. Sastry, Pepsin-gold colloid conjugates: preparation, characterization, and enzymatic activity, Langmuir 17 (2001) 1674–1679.
[54] A. Gole, C. Dash, C. Soman, S.R. Sainkar, M. Rao, M. Sastry, On the preparation, characterization, and enzymatic activity of fungal protease–gold colloid bioconjugates, Bioconjug. Chem. 12 (2001) 684–690.
[55] A.L. Crumbliss, S.C. Perine, J. Stonehuerner, K.R. Tubergen, J. Zhao, R.W. Henkens, J.P. O'Daly, Colloidal gold as a biocompatible immobilization matrix suitable for the fabrication of enzyme electrodes by electrodeposition, Biotechnol. Bioeng. 40 (1992) 483–490.
[56] J.H. Lin, W.L. Tseng, A method for fluorescence sensing of adenosine and alkaline phosphatase based on the inhibition of S-adenosylhomocysteine hydrolase activity, Biosens. Bioelectron. 41 (2013) 379–385.
[57] M.F. Cabral, L.F. Sgobbi, E.M. Kataoka, S.A.S. Machado, On the behavior of acetylcholinesterase immobilized on carbon nanotubes in the presence of inhibitors, Colloids Surf. B 111 (2013) 30–35.
[58] L. Bahari, Y. Gilad, I. Borovok, H. Kahel-Raifer, B. Dassa, Y. Nataf, Y. Shoham, R. Lamed, E.A. Bayer, Glycoside hydrolases as components of putative carbohydrate biosensor proteins in *Clostridium thermocellum*, J. Ind. Microbiol. Biotechnol. 38 (2011) 825–832.
[59] J.H. Lee, J.Y. Park, K. Min, H.J. Cha, S.S. Choi, Y.J. Yoo, A novel organophosphorus hydrolase-based biosensor using mesoporous carbons and carbon black for the detection of organophosphate nerve agents, Biosens. Bioelectron. 25 (2010) 1566–1570.
[60] J.S. Rudra, K. Dave, D.T. Haynie, Antimicrobial polypeptide multilayer nanocoatings, J. Biomater. Sci. Polym. Ed. 17 (2006) 1301–1315.
[61] R.C. Davies, A. Neuberger, B.M. Wilson, The dependence of lysozyme activity on pH and ionic strength, Biochim. Biophys. Acta 178 (1969) 294–305.
[62] C.H. Vannoy, J. Xu, R.M. Leblanc, Bioimaging and self-assembly of lysozyme fibrils utilizing CdSe/ZnS quantum dots, J. Phys. Chem. C 114 (2010) 766–773.
[63] J. Wang, E.R. Kantrowitz, Trapping the tetrahedral intermediate in the alkaline phosphatase reaction by substitution of the active site serine with threonine, Protein Sci. 15 (2006) 2395–2401.
[64] W. Khalid, G. Gobel, D. Huhn, J.M. Montenegro, P. Rivera-Gil, F. Lisdat, W.J. Parak, Light triggered detection of aminophenyl phosphate with a quantum dot based enzyme electrode, J. Nanobiotechnol. 9 (2011) 46.
[65] H. Soreq, S. Seidman, Acetylcholinesterase—new roles for an old actor, Nat. Rev. Neurosci. 2 (2001) 294–302.
[66] V. Pardo-Yissar, E. Katz, J. Wasserman, I. Willner, Acetylcholine esterase-labeled CdS nanoparticles on electrodes: photoelectrochemical sensing of the enzyme inhibitors, J. Am. Chem. Soc. 125 (2003) 622–623.
[67] K. Hofmann, G. Titus, J.A. Montibeller, F.M. Finn, Avidin binding of carboxyl-substituted biotin and analogs, Biochemistry 21 (1982) 978–984.
[68] F.M. Finn, G. Titus, K. Hofmann, Ligands for insulin receptor isolation, Biochemistry 23 (1984) 2554–2558.
[69] D. Shugar, The measurement of lysozyme activity and the ultra-violet inactivation of lysozyme, Biochim. Biophys. Acta 8 (1952) 302–309.
[70] P.C. Weber, D.H. Ohlendorf, J.J. Wendoloski, F.R. Salemme, Structural origins of high-affinity biotin binding to streptavidin, Science 243 (1989) 85–88.
[71] S. Pathak, M.C. Davidson, G.A. Silva, Characterization of the functional binding properties of antibody conjugated quantum dots, Nano Lett. 7 (2007) 1839–1845.
[72] B. Sahoo, M. Goswami, S. Nag, S. Maiti, Spontaneous formation of a protein corona prevents the loss of quantum dot fluorescence in physiological buffers, Chem. Phys. Lett. 445 (2007) 217–220.
[73] W. Bucking, S. Massadeh, A. Merkulov, S. Xu, T. Nann, Electrophoretic properties of BSA-coated quantum dots, Anal. Bioanal. Chem. 396 (2010) 1087–1094.
[74] B.J. Nehilla, T.Q. Vu, T.A. Desai, Stoichiometry-dependent formation of quantum dot-antibody bioconjugates: a complementary atomic force microscopy and agarose gel electrophoresis study, J. Phys. Chem. B 109 (2005) 20724–20730.
[75] E.A. Bayer, H. Ben-Hur, M. Wilchek, Isolation and properties of streptavidin, Methods Enzymol. 184 (1990) 80–89.